

Fermi Arcs in the Superconducting Clustered State for Underdoped Cuprates

G. Alvarez¹ and E. Dagotto²

¹*Computer Science & Mathematics Division and Center for Nanophase Materials Sciences,
Oak Ridge National Laboratory, Oak Ridge, TN 37831*

²*Department of Physics and Astronomy, University of Tennessee, Knoxville, Tennessee 37996, USA, and
Materials Science and Technology Division, Oak Ridge National Laboratory, Oak Ridge, Tennessee 32831, USA*

The one-particle spectral function of a state formed by superconducting (SC) clusters is studied via Monte Carlo techniques. The clusters have similar SC amplitudes but randomly distributed phases. This state is stabilized by the competition with antiferromagnetism, after quenched disorder is introduced. Fermi arcs between the critical temperature T_c and the cluster formation temperature scale T^* are observed, similarly as in the pseudogap state of the cuprates. The arcs originate at metallic regions in between the neighboring clusters that present large SC phase differences.

Introduction. Research in hole-doped high temperature superconductors is currently mainly focusing on the pseudogap (PG) phase that exists above T_c in the underdoped regime. This exotic phase acts as the normal state to superconductivity in a broad range of hole densities, and it may contain the solution to the puzzling properties of these compounds. Two groups of experiments have recently provided important microscopic information about the PG phase: (i) Using angle-resolved photoemission (ARPES) techniques [1], the PG Fermi surface was found to be composed of disconnected segments, widely known as “Fermi arcs” [2], that are centered at the nodal (N) points $\mathbf{k}=(\pm\pi/2, \pm\pi/2)$, in the usual two-dimensional (2D) square-lattice notation. These arcs are caused by the low-energy PG, which presents a \mathbf{k} -dependence resembling a d -wave SC gap close to the anti-nodal (AN) points $(0, \pm\pi), (\pm\pi, 0)$ [1], but it has gapless excitations in a finite momentum range near the nodes [3, 4]. The AN gaps remain approximately constant in the PG phase, in contrast with mean-field theories [3, 4]. (ii) Using scanning tunneling microscopy (STM) techniques, remarkable results were recently reported [5]. At temperatures well above T_c , the B2212 local density-of-state (LDOS) still closely resembles that of a d -wave superconductor. E.g., at optimal doping and $T=120\text{K}$, a d -wave gap is observed in clusters that appear to be randomly distributed [6].

Theoretically, the PG state is believed to be either (i) a precursor of the SC state, with phase fluctuations destroying superconductivity in an homogeneous state made out of small Cooper pairs formed by a strong attraction [7], or (ii) caused by other competing orders. However, a third possibility was recently proposed [8]. Via Landau-Ginzburg (LG) calculations, a state with nano-scale SC and antiferromagnetic (AF) clusters is stabilized when quenched disorder (caused, e.g., by chemical doping) influences on an otherwise homogeneous state with local coexistence of the SC and AF order parameters. The SC amplitude is robust and approximately the same in all the SC clusters. However, the phase of the SC order parameter, while uniform within each SC cluster, randomly changes from cluster to cluster causing the overall state to become non-SC. This scenario is concep-

tually different from (i) and (ii), but contains elements of both: the AF competing order is needed for the SC clusters to form and, once formed, phase fluctuations between clusters, occurring even in a weak-coupling BCS regime, destroy the SC condensate. This “Superconducting Clustered State” (SCCS) can account, at least qualitatively, for the STM experiments [5], since both are based on a similar inhomogeneous distribution of SC gaps above T_c . In this manuscript, it is shown that the SCCS also produces a Fermi surface (FS) with Fermi arcs.

LG simulations. Our calculations start with a LG theory for the AF vs. d -wave SC competition, studied with Monte Carlo (MC) techniques. Details were extensively discussed before [8] and only a brief summary will be repeated here. The LG classical Hamiltonian involves a complex number $\Delta_{\mathbf{i}}=|\Delta_{\mathbf{i}}|e^{i\phi_{\mathbf{i}}}$ and a real vector $\mathbf{S}_{\mathbf{i}}$, representing the SC and AF order parameters at site \mathbf{i} of a 2D square lattice. The interactions are the standard: 1. terms with up to 4th powers of the order parameters, locally favoring SC and AF; 2. nearest-neighbor (NN) couplings that spread the range of the order, emerging from gradients in the continuum formulation; and 3. an interaction between the order parameters, with strength $u_{\text{SC|AF}}$. Quenched disorder is also included to represent chemically doped cuprates. More specifically,

$$\begin{aligned}
 H = & r_{\text{SC}} \sum_{\mathbf{i}} |\Delta_{\mathbf{i}}|^2 + \frac{u_{\text{SC}}}{2} \sum_{\mathbf{i}} |\Delta_{\mathbf{i}}|^4 \\
 & + \sum_{\mathbf{i}, \alpha} \rho_{\text{AF}}(\mathbf{i}, \alpha) \mathbf{S}_{\mathbf{i}} \cdot \mathbf{S}_{\mathbf{i}+\alpha} + u_{\text{SC|AF}} \sum_{\mathbf{i}} |\Delta_{\mathbf{i}}|^2 |\mathbf{S}_{\mathbf{i}}|^2 \\
 & + \sum_{\mathbf{i}, \alpha} \rho_{\text{SC}}(\mathbf{i}, \alpha) |\Delta_{\mathbf{i}}| |\Delta_{\mathbf{i}+\alpha}| \cos(\phi_{\mathbf{i}} - \phi_{\mathbf{i}+\alpha}) \\
 & + r_{\text{AF}} \sum_{\mathbf{i}} |\mathbf{S}_{\mathbf{i}}|^2 + \frac{u_{\text{AF}}}{2} \sum_{\mathbf{i}} |\mathbf{S}_{\mathbf{i}}|^4. \tag{1}
 \end{aligned}$$

Previous investigations [8] showed that fixing, e.g., $r_{\text{SC}} = -1$, $r_{\text{AF}} = -0.85$, $u_{\text{SC}} = u_{\text{AF}} = 1$, $u_{\text{SC|AF}} = 0.7$ and varying ρ_{SC} and ρ_{AF} along the line $\rho_{\text{AF}} = 1 + \rho_{\text{SC}}$, produces a clean-limit phase diagram with a SC+AF region of local coexistence [8]. Fig. 1a qualitatively illustrates this clean limit case ($D=0$) [10]. However, quenched disorder $D \neq 0$,

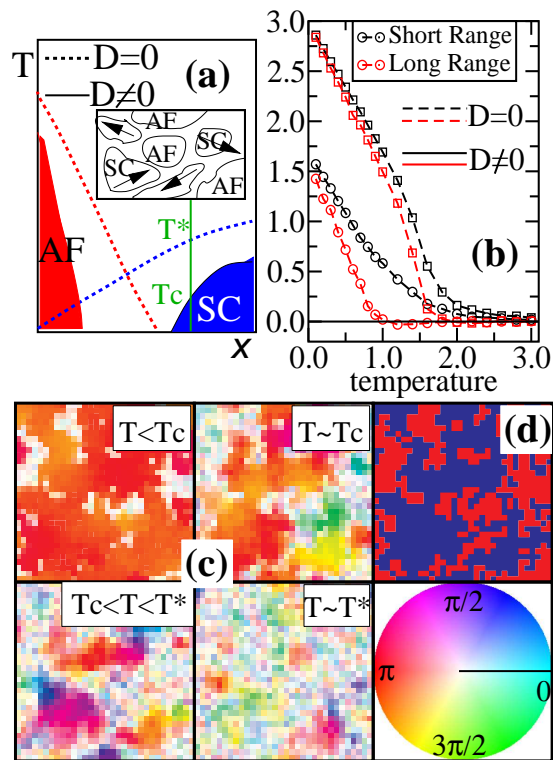


FIG. 1: (Color online) (a) Schematic T vs. doping (x) phase diagram [8] for the competition AF vs. SC: $D=0$ ($D \neq 0$) is the clean (dirty) limit. The vertical (green) line is the T -range emphasized here: at T_c long-range order develops, and at T^* SC clusters (short-range order) are formed. In practice, the AF to SC transition is reached in Eq.(1) by varying ρ_{SC} and ρ_{AF} , keeping $\rho_{AF}=1+\rho_{SC}$ for simplicity [8]. The disorder in the couplings is *correlated* with power $\alpha=0.8$ [9]. (b) SC correlation (SS) vs. T at short (vectorial distance (3,0)) and long (vectorial distance (16,16)) distance, in the clean and dirty limits. Results are from MC simulations on a 32×32 cluster with periodic boundary conditions, using 2,000 (3,000) thermalization (measurement) steps, starting with a random initial configuration. ρ_{SC} was taken from a bimodal distribution with values -1.1 and -0.1 in the dirty limit, and uniformly -1.1 in the clean limit. SS is defined as $SS(\mathbf{i}) = \frac{1}{N_{sites}} \sum_j |\Delta_j| |\Delta_{j+i}| \cos(\phi_j - \phi_{j+i})$. Some results gathered on 64×64 lattices show that size effects are not important. (c) Classical SC order parameter Δ for a typical MC-equilibrated configuration at several T 's (0.2, $1.0 \sim T_c$, 1.5 and $2.0 \sim T^*$). Color intensity represents $|\Delta|$ and the actual colors represent the SC angle ϕ at each site (see color wheel). The maximum value of $|\Delta|$ for the temperatures studied was ~ 2.0 . The bimodal couplings configuration is also shown (d): blue indicates regions where SC couplings dominate ($\rho_{SC} = -1.1$); red where AF couplings dominate ($\rho_{SC} = -0.1$).

for example introduced in Eq.(1) via a random distribution of ρ_{SC} and ρ_{AF} values, reduces both critical temperature, opening a gap between the competing phases. In this glassy region, nano-scale SC and AF clusters coexist, as sketched in the inset [8]. Two temperature scales emerge naturally: upon cooling, first the SC amplitude

develops at a crossover scale T^* , but the SC phases between clusters remain random. Reducing T further, coherence among the cluster phases is reached at T_c . The presence of two temperature scales is indeed observed numerically, as shown in Fig.1b: at $D=0$, the long and short correlations are very similar, while with disorder $D \neq 0$, a substantial difference between T^* and T_c (defined by the T where short and long range correlations vanish, respectively) is clearly observed. MC-equilibrated configurations of Eq.(1) better clarify this issue (Fig. 1c). The complex-number SC order parameters are represented by a color and an intensity (see wheel in Fig. 1c). At low T , the uniform and intense color indicates a robust SC state. As T increases, phase fluctuations appear near T_c . In the interesting range $T_c < T < T^*$, both SC clusters with random phases and non-SC (white) regions coexist: this is the SCCS emphasized here [11]. Finally, near T^* or above, few vestiges of SC remain.

Fermions in the SC+AF background. After equilibrated configurations of the SCCS state are gathered from the LG/MC classical analysis, fermionic properties are obtained by locally coupling itinerant electrons (simulating carriers) to the classical order parameters, as previously discussed [8]. The Hamiltonian is:

$$H_F = -t \sum_{\langle ij \rangle, \sigma} (c_{i\sigma}^\dagger c_{j\sigma} + H.c.) + 2 \sum_i J_i S_i^z s_i^z + \frac{1}{2} \sum_{i,\alpha} V_i |\Delta_{i\alpha}|^2 - \sum_{i,\alpha} V_i (\Delta_{i\alpha} c_{i\uparrow}^\dagger c_{i+\alpha\downarrow} + H.c.), \quad (2)$$

where $c_{i\sigma}$ are fermionic operators, $s_i^z = (n_{i\uparrow} - n_{i\downarrow})/2$ [12], $n_{i\sigma}$ is the number operator, and $\Delta_{i\alpha} = \beta |\Delta_{\mathbf{i}}| e^{i\phi_{\mathbf{i}}}$ are complex numbers for the SC order parameter defined now at the links $(\mathbf{i}, \mathbf{i}+\alpha)$ ($\alpha = \text{unit vector along the } x \text{ or } y \text{ directions; } \beta = 1 \text{ (-1) for } \alpha \text{ along } x \text{ (} y \text{)}$). For each $\{\Delta_{i\alpha}\}$ and $\{S_i^z\}$ configuration, the fermionic sector is exactly diagonalized via library subroutines and any property, static or dynamic, can be easily obtained. At $J_i = 0$, d -wave SC is favored since the pairing term involves NN sites, as in any standard mean-field Bogoliubov-de-Gennes (BdG) approximation [13]. The parameters of relevance are J_i and V_i (t is the energy unit), and they carry a site dependence to easily include quenched disorder [14].

Fermi arcs. Fig. 2 contains our most important results. (a) shows the one-particle spectral function $A(\mathbf{k}, \omega)$ along a straight line from the N to the AN points. At low $T < T_c$, the d -wave SC gap is clearly visible (higher $|\omega|$ peaks are related with a nodeless AF gap, and they do not affect lower energy features). However, as T is raised first across T_c , then through the intermediate SCCS phase-fluctuating regime proposed for the PG state, and finally to above T^* , clearly the gaps disappear forming segments (arcs) starting at the node, with a length that grows with increasing T . In (b), the FS's are shown: four nodes at low T become arcs at higher T , they eventually merge, and form a closed FS at the highest T . (c) contains an

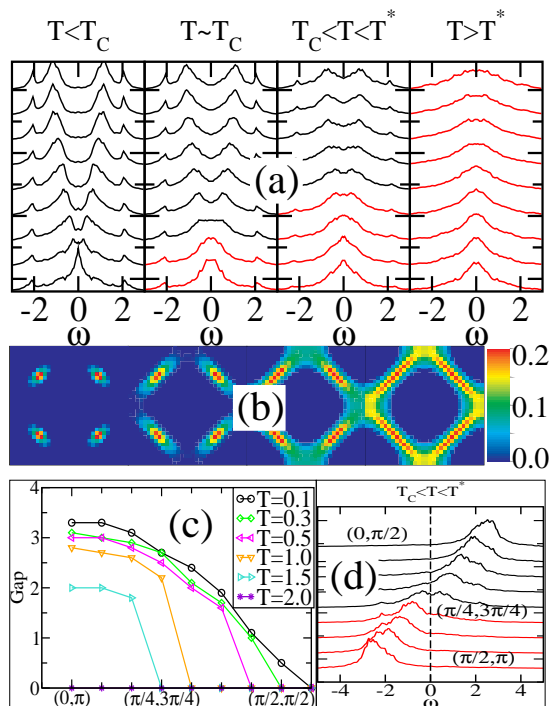


FIG. 2: (Color online) (a) $A(\mathbf{k}, \omega)$ for equally-spaced \mathbf{k} 's along the direction from $(\pi/2, \pi/2)$ (bottom) to $(0, \pi)$ (top). The classical LG configurations used are obtained as described in Fig. 1 but for the case $\rho_{SC} = -0.8$ (0) in the SC (AF) regions, using $\rho_{AF} = 1 + \rho_{SC}$, on a 32×32 lattice. The T 's are, from left to right, $T = 0.1, 0.4, 1.0$ and 2.0 . In this case, $T_c \sim 0.4$, and $T^* \sim 1.2-1.5$. (b) $A(\mathbf{k}, \omega = 0)$ in the k_x-k_y plane for the same parameters and temperatures as in (a). Results shown are those within a window $\Delta\epsilon = 0.1$ from the Fermi level. (c) SC gap (distance between peaks) vs. momentum for the same parameters as in (a) but with $\rho_{SC} = -1.1$ or -0.1 (bimodal distribution), at the T 's indicated. (d) $A(\mathbf{k}, \omega = 0)$ from $(0, \pi/2)$ to $(\pi/2, \pi)$, at $T = 1.0$ and parameters as in (a).

example of gaps vs. \mathbf{k} along the N-AN line, showing the arc formation, and the stability of the AN gap even when T is varied over a wide range. Here, as in [3, 4], a given \mathbf{k} is said to have a gap if two peaks are found in $A(\mathbf{k}, \omega)$. In Fig. 3a, the length of the Fermi arc is shown vs. T , and an approximate linear relation is found. All these results are in good agreement with ARPES [3, 4].

An important observation is that the arcs are *not* merely caused by the broadening of the peaks by disorder. To understand this, consider now the direction *perpendicular* to the N-AN line. In Fig. 2d, $A(\mathbf{k}, \omega)$ from $(0, \pi/2)$ to $(\pi/2, \pi)$ is shown. This crosses the N-AN line at $(\pi/4, 3\pi/4)$. The figure shows that in the range $T_c < T < T^*$ a *metallic* dispersion, close to non-interacting electrons, is observed. This is totally different from the low- T results that show a BdG quasiparticle dispersion and a gap (not shown). Concomitant with this behavior, by monitoring the LDOS in our simulations, we have noticed the existence of gapless metallic patches coexist-

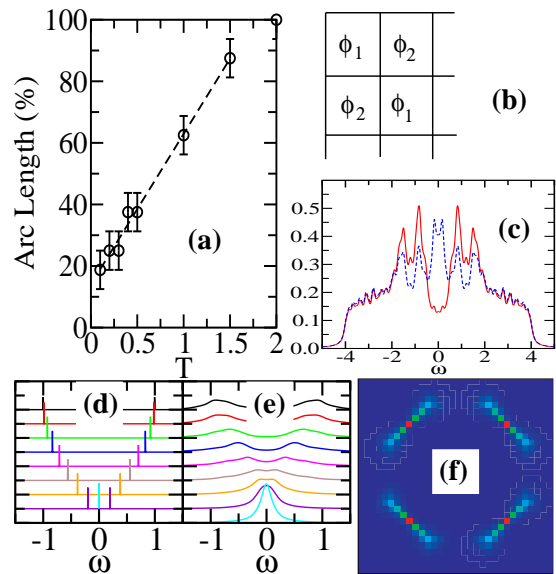


FIG. 3: (Color online) (a) Length of the Fermi arc (as a % of the maximum length) vs. T for the case described in Fig. 2a. The Fermi arc was defined to exist at a certain momentum \mathbf{k} when its intensity was within 35% of the maximum intensity. Other definitions lead to a similarly linear relation but with different $T \rightarrow 0$ limits. Note that the energy cutoff $\Delta\epsilon = 0.1$ and the finite momentum resolution, due to the lattice's finite size, prevent the size of the nodes from being exactly zero in the low- T state. If a shift downwards by 20% (the value at $T = 0$) is carried out, an even better agreement with [3, 4] is obtained. (b) Schematic representation of the toy model configuration (see text). ϕ_1 and ϕ_2 refer to the SC order parameter phases in 4×4 squares. (c) LDOS for the example shown in (b) with $\phi_1 = 0$ and $\phi_2 = \pi$. Red (blue) solid (dashed) lines correspond to a site at the center (border) of the 4×4 square. The parameters used are the same at each site: $|\Delta| = 1$, $V = 0.25$, and $J = 2$. (d) $A(\mathbf{k}, \omega)$ for \mathbf{k} along the direction $(\pi/2, \pi/2)$ to $(0, \pi)$ for the case shown in (b) with $\phi_1 = \phi_2 = 0$ (i.e. perfect d -wave superconductor). (e) Same as (d), but with ϕ_1 and ϕ_2 randomly chosen between 0 and π . (f) $A(\mathbf{k}, \omega = 0)$ in the k_x-k_y plane for case (e) ($\Delta\epsilon = 0.1$).

ing with the AF and SC clusters. These metallic regions appear in “fragile” zones of the disordered configuration, such as in long and thin areas of one phase penetrating into the other, where none of the two orders prevails. Thus, the SCCS actually involves three ingredients: SC, AF, and metallic areas. Our numerical simulations suggest that the metallic areas and Fermi arcs are related.

Toy models. To better understand the Fermi arc formation in the SCCS, simplified models were analyzed. Consider a 2D square lattice regularly divided into smaller 4×4 squares (Fig. 3b), all with the same SC amplitude but different phases, and without AF. To simulate T effects, frozen configurations $\{\phi\}$ of the SC phases were studied. In Fig. 3d, the uniform case $\phi_1 = \phi_2 = 0$ is shown: as expected, a clear d -wave gap exists along the N-AN line. This mimics the regime $T < T_c$ in Fig. 2a. To simulate $T_c < T < T^*$, consider now a *random* distribution

of phases. The result (Fig. 3e) still shows a clear gap in the AN point, but near the nodal point now a finite set of momenta do *not* present a gap anymore, thus generating a Fermi arc (see also the FS in Fig. 3f)). Studying $A(\mathbf{k}, \omega)$ for a variety of ϕ_2 's, at fixed $\phi_1=0$, we observed that angles such that $\cos(\phi_2)<0$ are those that most contribute to the arcs. For, e.g., $\phi_2=\pi$ metallic portions were identified at the lines separating two domains (Fig. 3c) [15].

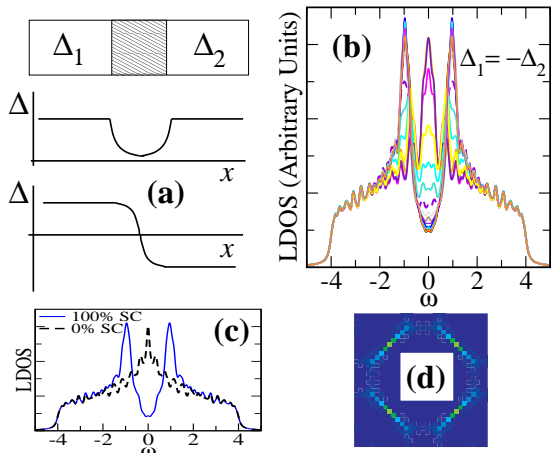


FIG. 4: (Color online) (a) Schematic representation of a Josephson-junction-like structure. Top: two SC regions with order parameters Δ_1 and Δ_2 , separated by a $\Delta=0$ area of width w (grey). Middle: expected gap interpolation due to proximity effect, for $\Delta_1=\Delta_2$. Bottom: same as middle, but for $\Delta_1=-\Delta_2$. (b) LDOS on a 32×32 lattice containing 4 equally-spaced 12×12 SC clusters separated by $w=4$. The order parameters are staggered between $\Delta_1=1$ and $\Delta_2=-1$, with $V=0.25$ and without AF ($J=0$). Shown are results from the center of one SC region to a nearest-neighbor. (c) Density of states of a perfect superconductor (blue solid) and of a perfect metal (black dashed) on a 32×32 lattice. Note the Van Hove singularity in the 2D metal. (d) $A(\mathbf{k}, \omega=0)$ in the k_x-k_y plane for $\Delta_1=-\Delta_2=1$ and $w=2$, with a setup as described in (b) but using 14×14 SC clusters.

Relevance of large phase differences. The metallic regions seem caused, at least in part, by large phase differences between neighboring SC clusters. Consider Fig. 4a: here two SC clusters are shown, with order parameters $\Delta_1 \neq 0$ and $\Delta_2 \neq 0$, separated by an intermediate thin region where $\Delta=0$. If $\Delta_1=\Delta_2$, this intermediate region will develop a gap by proximity effect (Fig. 4a), and the FS has still 4 nodes, as confirmed by an explicit BdG calculation (not shown). However, if $\Delta_1=-\Delta_2$ a qualitative difference occurs: now the interpolation in the intermediate region necessarily requires the existence of a zero, where the SC order parameter must vanish even for a thin $\Delta=0$ layer (Fig. 4a). A BdG study confirms that the LDOS in the middle between two “anti-parallel” SC clusters is almost identical to the LDOS of a metallic state (see Figs. 4b,c). The FS for $\Delta_1=-\Delta_2$ has Fermi arcs (Fig. 4d). Thus, large ϕ differences induce metallic regions, and those appear to cause the Fermi arcs.

Conclusions. A state based on SC clusters with random phases was here used to calculate the ARPES response of the PG state. Fermi arcs were found in a T range between T_c and the T^* where the clusters start forming upon cooling. Toy models illustrate and simplify these results. For further progress, our effort must be supplemented by better analytic control of the SCCS and by numerical studies using microscopic models. The extension of these results to s -wave superconducting films should also be pursued [16]. In addition, the STM experiments [5] not only showed a clustered state in a broad temperature range, but also unveiled a regime immediately above T_c where 100% of the sample had the d -wave gap. Adapting the SCCS to also accommodate this feature will require increasing the attraction V [17] and this direction will be the focus of future investigations.

Work supported by the NSF grant DMR-0706020, the Division of Materials Science and Engineering, U.S. DOE, under contract with UT-Battelle, LLC, and by the CNMS, sponsored by the Scientific User Facilities Division, BES-DOE.

- [1] A. Damascelli *et al.*, Rev. Mod. Phys. **75**, 473 (2003).
- [2] M. Norman *et al.*, Nature **392**, 157 (1998).
- [3] A. Kanigel *et al.*, Nature Physics **2**, 447 (2006).
- [4] A. Kanigel *et al.*, Phys. Rev. Lett. **99**, 157001 (2007).
- [5] K. Gomes *et al.*, Nature **447**, 569 (2007).
- [6] This is compatible with Nernst experiments (Y. Wang *et al.*, Phys. Rev. B **73**, 024510 (2006)), and μ -SR measurements (J. Sonier *et al.*, arXiv:0801.3481).
- [7] M. Randeria *et al.*, Phys. Rev. Lett. **69**, 2001 (1992); V. J. Emery and S. A. Kivelson, Nature **374**, 434 (1995).
- [8] G. Alvarez *et al.*, Phys. Rev. B **71**, 014514 (2005); M. Mayr *et al.*, Phys. Rev. B **73**, 014509 (2006).
- [9] H. Makse *et al.*, Phys. Rev. E **53**, 5445 (1996).
- [10] Experimental evidence is accumulating that a glassy state should not be present in the real cuprate’s clean limit phase diagram (F. Rullier-Albenque *et al.*, arXiv:0710.3737 and [8]), as also found in manganites (E. Dagotto, Science **309**, 257 (2005)).
- [11] Figure 1c emphasizes one quenched disorder configuration, but calculations have been repeated for several other configurations and they are all qualitatively similar.
- [12] We use Ising spin degrees of freedom (d.o.f.). Studies with Heisenberg d.o.f. lead to qualitatively similar conclusions, but they are more CPU time consuming.
- [13] In the limit $T \rightarrow 0$, the BdG equations (W. A. Atkinson *et al.*, Phys. Rev. B **68**, 054501 (2003)), supplemented by a competing AF interaction, are recovered. For simplicity, the chemical potential is chosen as $\mu=0$ (density $n=1$) for both the AF and SC clusters. Reducing n to values such as $n=0.9$ does not alter our conclusions, but increases the simulation’s complexity due to μ tuning.
- [14] Our convention was to choose $V=-0.25\rho_{SC}$ (0) at the sites where $\rho_{SC}<0$ (>0). Intuitively, in the blue sites of Fig. 1d, the SC attraction is strong and in the red ones, it is weak. Reciprocally, $J=2.0\rho_{AF}$ (0) if $\rho_{AF}>0$ (<0).

- [15] Sub-gap states exist in d -wave SC π -interfaces (A. Martin and J. Annett, cond-mat/9910208).
- [16] A. Goldman and N. Marković, Phys. Today **51** (11), 39 (1998); A. Ghosal *et al.*, Phys. Rev. B **65**, 014501 (2001);
- Y. Dubi *et al.*, Nature **449**, 876 (2007).
- [17] M. Mayr *et al.*, Phys. Rev. Lett. **94**, 217001 (2005).